CLIMATOLOGY

Strong links between Saharan dust fluxes, monsoon strength, and North Atlantic climate during the last 5000 years

Juncal A. Cruz[1], Frank McDermott[2], María J. Turrero[3], R. Lawrence Edwards[4], Javier Martín-Chivelet[1,5]*

Despite the multiple impacts of mineral aerosols on global and regional climate and the primary climatic control on atmospheric dust fluxes, dust-climate feedbacks remain poorly constrained, particularly at submillennial time scales, hampering regional and global climate models. We reconstruct Saharan dust fluxes over Western Europe for the last 5000 years, by means of speleothem strontium isotope ratios ($^{87}Sr/^{86}Sr$) and karst modeling. The record reveals a long-term increase in Saharan dust flux, consistent with progressive North Africa aridification and strengthening of Northern Hemisphere latitudinal climatic gradients. On shorter, centennial to millennial scales, it shows broad variations in dust fluxes, in tune with North Atlantic ocean-atmosphere patterns and with monsoonal variability. Dust fluxes rapidly increase before (and peaks at) Late Holocene multidecadal- to century-scale cold climate events, including those around 4200, 2800, and 1500 years before present, suggesting the operation of previously unknown strong dust-climate negative feedbacks preceding these episodes.

INTRODUCTION

Desert dust aerosols affect Earth's global energy balance in multiple ways, including by scattering and absorbing radiation, modifying cloud albedo and lifetime, and affecting the carbon cycle by ecosystem fertilization (*1*). Also, they regionally affect the water cycle by influencing cloud formation and precipitation (*2*) and affect human health through air pollution (*3*). On a global scale, the largest source of mineral dust for the atmosphere is located in the northern African desert, from where huge amounts of dust are exported continuously (but not steadily) via the atmosphere over the Atlantic Ocean and the Mediterranean (*4*). Understanding dust-climate relationships is a major scientific challenge for climate modeling (*5*, *6*) and, despite notable advances, considerable uncertainties remain because of the number and complexity of processes that affect radiative fluxes. Difficulties are further aggravated because atmospheric dust fluxes vary at all temporal scales and can be difficult to quantify at climate-relevant time scales. Saharan dust fluxes show strong interannual and interdecadal variability (*7*), both of which influence and are affected by a multitude of regional-scale processes. Some recent work on Mediterranean and north African lake records (*8*–*10*), European ice cores (*11*), and Atlantic sediments (*12*–*16*) indicate considerable variability also at longer time scales. Despite these advances, our knowledge on dust changes occurring at centennial to millennial time scales is still very limited and strongly hampers robust quantitative evaluation of desert dust–climate feedbacks.

In this work, supradecadal- to millennial-scale changes in Saharan dust fluxes during the Late Holocene [4.9 to 0.9 ka (thousand years) before the present (BP)] are reconstructed using an innovative speleothem-based paleodust proxy. Specifically, we present a quantitative estimation of Saharan dust deposition rates that occurred in southwestern continental Europe (43°N), a region located >2000 km north of Saharan dust sources. Our paleodust reconstruction is based on strontium isotopic ratios ($^{87}Sr/^{86}Sr$) measured in speleothem calcite (cave deposits). The study focuses on variations in $^{87}Sr/^{86}Sr$ ratios along a uranium series–dated stalagmite retrieved from Kaite Cave (northern Spain) (fig. S1). Inference of paleodust fluxes using Sr isotopic ratios was based on characterization and modeling of the present-day cave geochemical system for $^{87}Sr/^{86}Sr$ ratios, including cave drip waters and speleothems, as well as different sources of strontium including cave host rock, sea salt aerosols, and Saharan dust. Our results provide key data for understanding mid- and long-term Saharan dust flux patterns and quantifying dust-climate relationships during the Late Holocene. They also offer a robust new dust-flux time series as an input for climate models.

An area prone to dust deposition in Western Europe

The northern part of the Iberian Peninsula is a key region for understanding past climate dynamics because of its location between the North Atlantic, the Mediterranean, northwestern Africa, and northwestern Europe. The area is characterized in the present day by Saharan dust deposition fluxes in the range of 4.4 ± 1.1 g m^{-2} year^{-1} (see Materials and Methods).

Dust fluxes in this area are linked to Saharan dust outbreaks from northern Africa, which typically occur several times per year (*17*), with the main sources found in southern Algeria and northern Mali region, and in the western coast of northern Africa (Western Sahara, western Mauritania, and Atlas foothills) (*18*, *19*), although other, more distant Saharan areas can also act as primary sources of dust (*20*). In the dust source areas (Fig. 1), large quantities of dust are injected into the atmosphere by resuspension and are transported toward Iberia under diverse synoptic atmospheric scenarios. During summer, these scenarios are dominated by a strong North African high at the upper levels, whereas, for the rest of the year, they are commonly controlled by a North African high at surface levels or by an Atlantic low located west of Iberia (*19*). Interdecadal patterns of dust influxes over Spain during the instrumental period reflect the

[1]Department of Geodynamics, Stratigraphy, and Paleontology, Faculty of Geological Sciences, Complutense University of Madrid, Madrid, Spain. [2]UCD School of Earth Sciences and Earth Institute, University College Dublin, Belfield, Dublin 4, Ireland. [3]Centro de Investigaciones Energéticas, Medioambientales y Tecnológicas (CIEMAT), Madrid, Spain. [4]Department of Earth Sciences, University of Minnesota, Minneapolis, MN, USA. [5]Institute of Geosciences IGEO (CSIC-UCM), José Antonio Novais, 12 Madrid, Spain.
*Corresponding author. Email: martinch@ucm.es

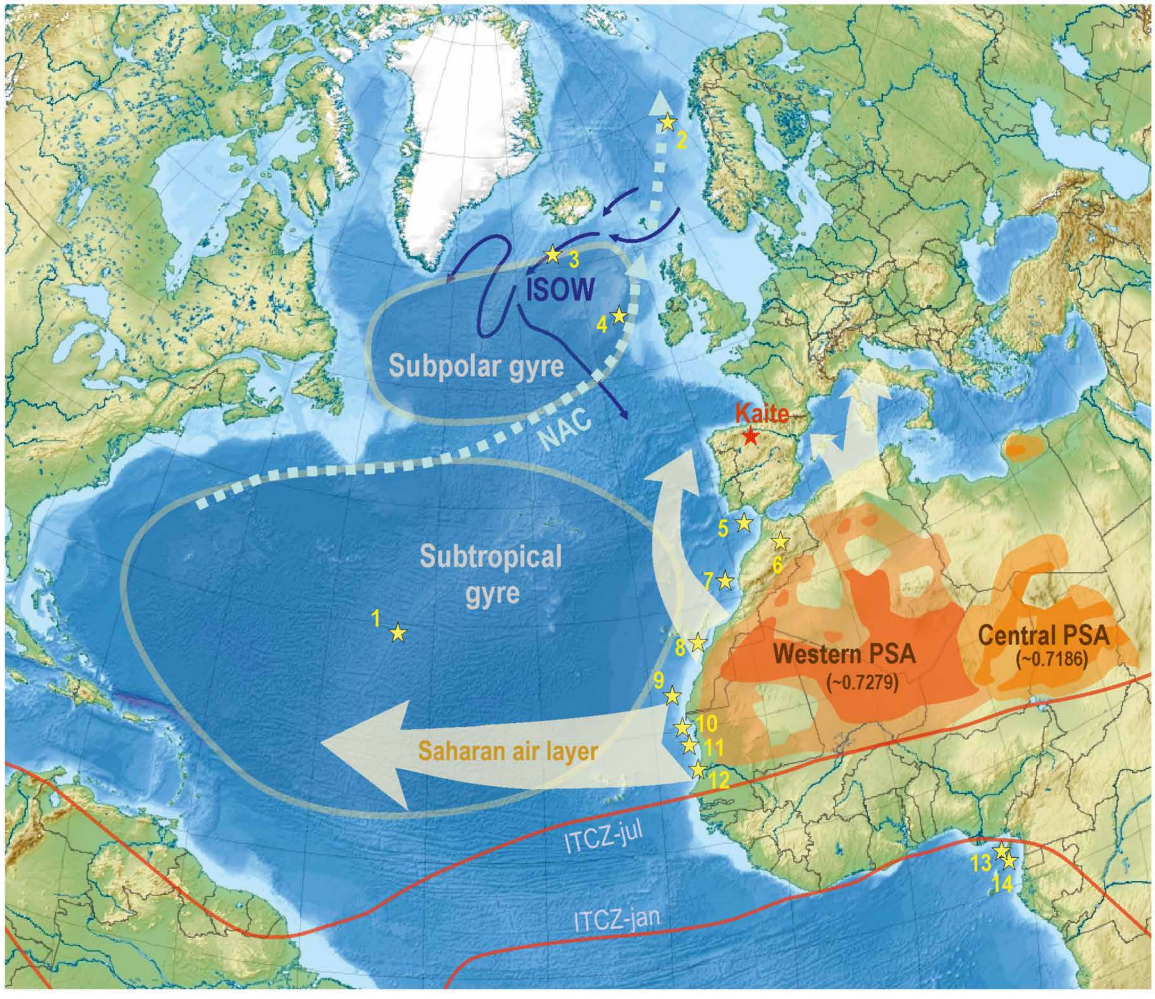

Fig. 1. Kaite paleodust record in the context of the North Atlantic region. Map showing the location of the site for the dust flux reconstruction based in stalagmite Buda-100 (Kaite Cave, northern Spain), indicated with a red star, as well as of other previous proxy reconstructions mentioned in this paper (yellow stars, numbered 1 to 11): (1) Mid-Atlantic dust flux record, GGC6 sediment core (*13*); (2) North Atlantic Current (NAC) temperature record, MD95-2011 sediment core (*48*); (3) Iceland-Scotland Overflow Water (ISOW) strength record, GS06-144 08GC sediment core (*51*); (4) NAC drift ice record, VM-29-191 sediment core (*61*); (5) Gulf of Cadiz hydroclimate reconstruction, GeoB5901-2 core site (*53*); (6) Sidi Ali lake (Morocco) paleoprecipitation and paleodust record (*10*); (7) Eastern North Atlantic Central Water offshore Morocco temperature record, OC437-7 24GGC sediment core (*46*); (8) GC37 sediment core near Canary Islands (*34*); (9) OC437-7/GC49 sediment core, offshore Western Sahara (*12*); (10) dust record, GeoB9501 sediment core (*14*); (11) dust record, ODP-658C (*15*); (12) dust record, OC437-7/GC68 sediment core, offshore Mauritania (*12*); (13) Sahel-Sahara paleoprecipitation record, GeoB4905-4 sediment core (*35*); (14) Gulf of Guinea sea surface temperature, MD03-2707 sediment core (*39*). The map also includes the dominant Saharan dust trajectories toward Western Europe and the North Atlantic (*18*, *19*). Western PSA and Central PSA indicate the North African dust "preferential source areas" and their approximate average values for dust $^{87}Sr/^{86}Sr$ (in parentheses) (*20*).

changes occurring at the African dust source areas and are comparable to those detected in northwestern Africa and the Atlantic (see fig. S2).

Our study site is Kaite Cave (Ojo Guareña Karst Natural Monument, 43°2′ N, 3°39′ W; 870 m above sea level), a small, poorly ventilated, superficial cave located to the south of the Cantabrian Mountains, northern Spain (Fig. 1 and Materials and Methods). The cave is hosted in a massive limestone of Late Cretaceous age. This lithological unit forms the caprock of a low dipping cuesta, and the cave is located near the top of the ridge. At the surface, the cave site shows quite flat orography, determined by the gentle backslope of the cuesta, moderate cover of bush type vegetation, and a very thin, immature lithosol, which consists of weathered host rock and aeolian fine material. The site, which has no relevant surface runoff, is prone to dust accumulation, which takes place mostly by wet deposition (precipitation scavenging), while "dry" deposition (not involving an aqueous phase) is clearly subordinated (*21*). Over the cave, there is no other possible source of sediment besides the atmosphere and the weathered limestone itself.

The present-day climate of the area is warm temperate, averaging 10°C, with both Atlantic (oceanic) and Mediterranean features. Annual precipitation, which is usually above 900 mm, is determined mainly by northern Atlantic mid-latitude storms (polar front low-pressure cells) with a marked Mediterranean seasonality with relatively dry and warm summers. Reconstructions of hydroclimate for the last millennia in the area (in part based on speleothems from Kaite, see fig. S3) reveal strong interannual variability but relatively minor changes in the bulk rainfall at decadal to millennial scales.

RESULTS

Speleothems are capable of yielding high-resolution paleorecords because of the following: (i) They grow gradually from cave drip waters whose hydrochemistry can change in response to environmental changes occurring outside the cave, and (ii) they can be precisely age-dated by uranium series methods and high-resolution microstratigraphy. Most speleothems consist of calcium carbonate, which can incorporate trace elements such as strontium, which substitutes for Ca in the calcite lattice during speleothem growth (*22*). Because strontium isotopes do not fractionate significantly from geological or biological processes, the $^{87}Sr/^{86}Sr$ ratio of speleothems can be used as a natural tracer of strontium sources (*23*–*27*). The $^{87}Sr/^{86}Sr$ ratio of precipitated calcite should be identical to that of the drip water from which it derives, which, in turn, reflects the multicomponent mixture of strontium with different isotopic ratios, each component determined by its provenance. These include both internal (cave host rock) and external (mineral dust and sea spray deposited above the cave) sources (see Materials and Methods).

Sr isotope measurements ($^{87}Sr/^{86}Sr$) were performed on 101 samples of calcite of a Late Holocene stalagmite from Kaite Cave (fig. S1), as well as on 20 additional samples comprising present-day calcite precipitates, drip waters, cave host rock, soil above the cave, and meteoric waters (table S1). The time series reconstruction was based on 15 radiometric (U-Th) age-dates, which allowed a high-resolution age model for the inferred changes in dust fluxes between 4.9 and 0.9 ka BP (table S2 and fig. S4). During this interval, the stalagmite grew vertically at remarkably steady rates, averaging 0.27 mm/year. Stalagmite $^{87}Sr/^{86}Sr$ ratios reveal consistent changes through time, including well-defined trends and patterns at supradecadal to millennial scales (Fig. 2).

Past rates of Saharan dust deposition have been calculated using a two-step model (see Materials and Methods). First, a mass balance model for $^{87}Sr/^{86}Sr$ ratios based on present-day measurements allowed calculation of the effect of inputs of Saharan dust on the $^{87}Sr/^{86}Sr$ ratios of speleothems currently growing in Kaite Cave, as well as effects of inputs from other sources (cave host rock and sea salt aerosols). Results show that cave rock is the main strontium contributor (~93.2%) to present-day speleothem strontium, followed by Saharan dust (~5.2%) with minor inputs from sea salt (~1.6%). Second, past dust deposition rates are forward modeled by calculating the changes in current conditions that are required to reproduce the past speleothem $^{87}Sr/^{86}Sr$ measurements.

Dust deposition rates inferred from stalagmite $^{87}Sr/^{86}Sr$ reveal substantial changes through time and show patterns that are consistent with previously published flux estimates (Fig. 3), although these have poorer temporal resolution or do not span the entire time interval reconstructed here. According to our data, dust deposition during the 4.9 to 0.9 ka BP interval never reached the current rate for northern Iberia, and past values ranged between 33 and 80% of today's value (Fig. 2). Lowest values are broadly coherent with dust deposition rates simulated by climate models for 6 ka BP (*28*–*30*), i.e., the so-called African Humid Period (AHP). During the AHP,

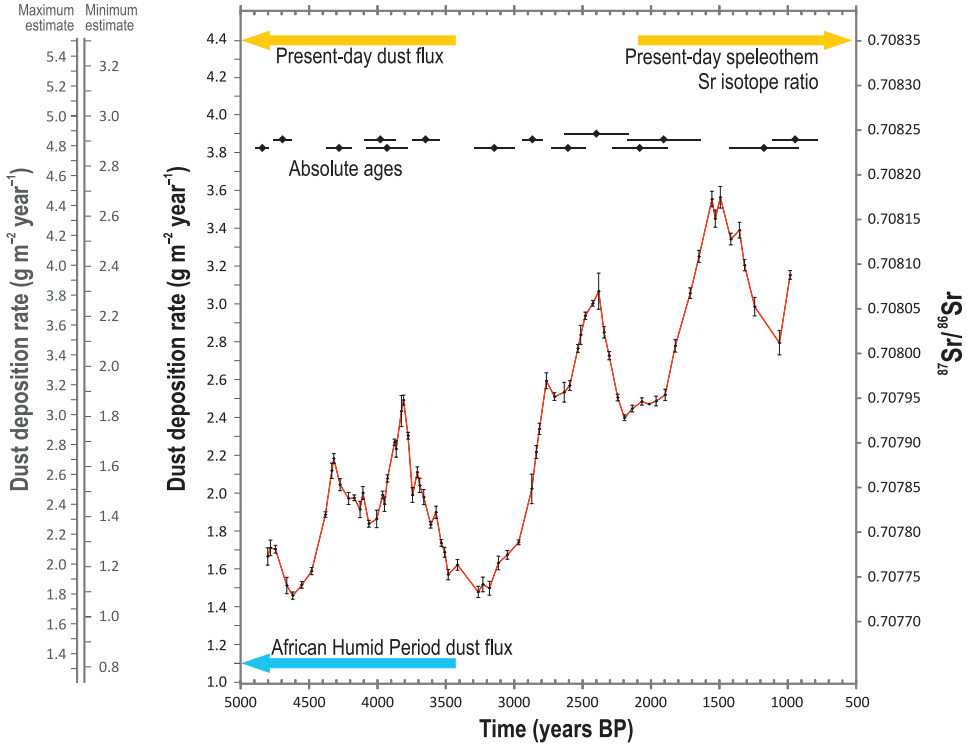

Fig. 2. Reconstruction of Saharan dust flux in northern Iberia. Dust deposition rate (left axis) based on $^{87}Sr/^{86}Sr$ ratios (right axis) measured along stalagmite Buda-100 from Kaite Cave (Spain) and U-Th age-dating, which allowed a high-resolution age model for 4.9 to 0.9 ka BP interval (horizontal axis). Two additional reconstructions for Saharan dust fluxes are given based on the lowest and highest estimates for present-day dust fluxes, and, respectively, in maximum and minimum estimates for average $^{87}Sr/^{86}Sr$ ratios of Saharan dust reaching the cave area (see the Supplementary Materials for details). The paleodust fluxes inferred from Buda-100 are always above of the deposition rates simulated for the so-called African Humid Period at ~6.0 ka BP (*28*, *29*) and below present-day values. Error bars are 2σ for both ^{230}Th ages and $^{87}Sr/^{86}Sr$ ratios.

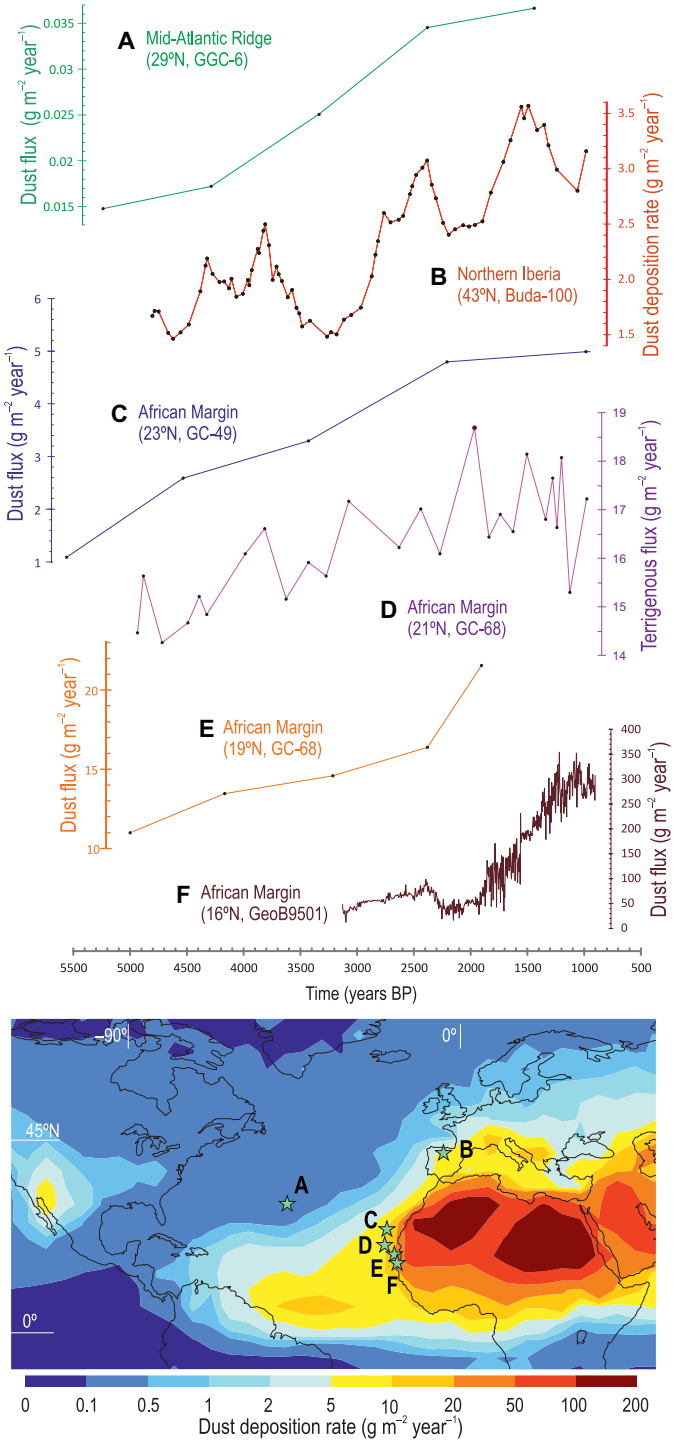

Fig. 3. Saharan dust in Iberia versus North Atlantic paleodust records. Dust reconstruction based in Buda-100 stalagmite compared with previous dust reconstructions based in marine sediment core GG6-C of the mid-Atlantic ridge (*13*) and sediment cores GC49 and GC68 (*12*), GeoB9501 (*14*), and ODP-658C (*15*) of the northwestern African margin. Beyond the different resolution of the records, all show good coherence in the long-term trend. Also, the absolute values of dust fluxes are concordant with the distance of the sampling sites to dust sources and pathways. The map shows current average dust deposition (*32*) rates and location of paleodust record sites.

Saharan dust fluxes probably reached the minimum values for the whole Holocene (*13*, *31*).

Compared with other previous Saharan dust paleorecords (Fig. 3), depositional rates calculated for Iberia are intermediate between those inferred for the northwestern African margin, which could be up to one order higher (*12*), and those calculated for the mid-Atlantic ridge (*13*), which are one order of magnitude lower. These intermediate values are broadly consistent with the distance to the main Saharan dust plume and present-day dust rates (*32*).

The main features of our paleodust record are as follows: (i) a long-term net increase in dust deposition for the whole time interval (4.9 to 0.9 ka BP), in which dust deposition rates change from very low values close to typical AHP ones to high rates approaching (but never reaching) present-day values; and (ii) a superimposed millennial-scale quasi-periodic pattern, defined by alternating intervals of low (4.7 to 4.6, 3.5 to 3.2, 2.3 to 1.9, and 1.3 to 1.0 ka BP) and high dust deposition rates (4.4 to 3.8, 2.9 to 2.4, and 1.8 to 1.4 ka BP), the latter with very remarkable peaks at 4.3, 3.8, 2.8, 2.4, and 1.5 ka BP.

DISCUSSION

Long-term Saharan dust increase

Our results reveal a progressive but nonlinear increase in Saharan dust deposition in northern Iberia between 4.9 and 0.9 ka BP (Fig. 2), an increase that probably started some centuries before, according to superregional dust reconstructions (*12*, *16*) and climate simulations (*28*, *29*), and that continues today, as indicated by present-day data from the studied cave. Such a net increase is consistent with the long-term desertification process experienced by northern Africa, including the Sahara and the Sahel, starting around 5.5 ka BP with the rapid demise of the AHP (~11.7 to 5 ka BP) (*33*–*35*), and continuing more gradually over the remainder of the Holocene (*13*). During these later millennia, the progressive aridification in northern Africa is reflected by lake levels (*8*, *36*), vegetation changes (*37*), human settlements (*38*), and dust fluxes over the northwest African margin (*12*, *14*, *15*, *33*) (Fig. 3); the latter was estimated to increase ~5-fold since the AHP (*12*). The long-term change in dust fluxes is probably related to progressive strengthening of the latitudinal temperature gradient (LTG) (Fig. 4D) in the Northern Hemisphere, in turn induced by a gradual increase in the latitudinal insolation gradient (LIG) (Fig. 4C) as insolation declined faster at high latitudes than at equatorial latitudes in response to orbital parameters. Stronger LIGs and LTGs produced weaker monsoon conditions in West Africa (*39*) that mimic the waning of East African, Indian Ocean, and Asian monsoon systems (*40*, *41*) (Fig. 4) and the gradual southward shift of the mean latitudinal position of the intertropical convergence zone in the Atlantic (*42*). The differential cooling of high northern latitudes with respect to equatorial regions also promoted a stronger Hadley circulation and a southward shift of the Azores high. In the mid-latitudes, the westerly flow increases, with enhanced moisture transport and precipitation over central and northern Europe (*43*), which contrasts with the broad aridification of northern Africa. Northern Iberia, located between those areas, did not experience substantial changes in precipitation in the long term, except a possible small net trend to drier conditions (*44*, *45*) (fig. S3). Our results suggest that long-term change in Saharan dust deposition is dominated by the strengthening of the sources.

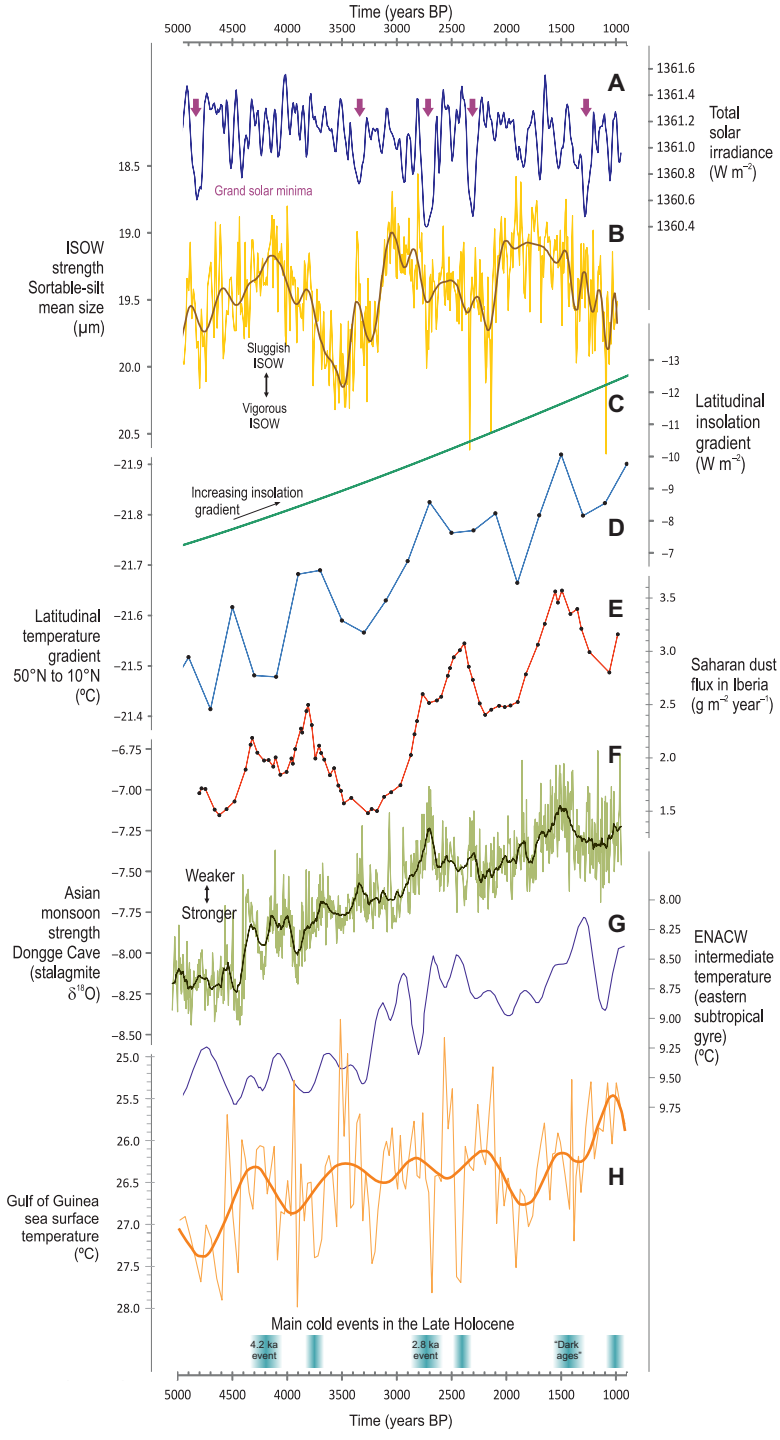

Fig. 4. Saharan dust fluxes and key ocean-atmosphere and climate time series. Time series for selected ocean-atmosphere proxy records (see Fig. 1 for locations) and for key climate forcings in the 4.9 to 0.9 ka BP interval. (**A**) Reconstruction of the total solar irradiance (*59*) with purple arrows indicating grand minima of solar activity. (**B**) Flow speed in the Iceland-Scotland overflow water (ISOW) inferred from sortable-silt mean size (average) in core GS06-144 08GC (*51*). Smooth curve is a B-Spline fit 10 dec. (**C**) LIG for 15 July in the Northern Hemisphere, given by the insolation between latitudes 65° and 15°N, using data from (*79*). (**D**) LTG for the Northern Hemisphere, between latitudes 50° and 10°N, calculated with data from (*43*) (40° to 60°N annual average temperature minus 0° to 20°N annual average temperature). (**E**) Saharan dust deposition rate in northern Iberia (this paper). (**F**) Strength of the Asian monsoon inferred from oxygen isotope ratios in a stalagmite from Dongge Cave, southern China (25°N, 108°E) (*40*). Smooth curve is a 24-point running mean. (**G**) Intermediate water temperature of the Eastern North Atlantic Central Water (ENACW) inferred from Mg/Ca in sediment core OC437-7 24GGC (*46*) located in the eastern boundary of the subtropical gyre. The curve is a 200-year low-pass filter. (**H**) Sea surface temperature in the Gulf of Guinea estimated by Mg/Ca of MD03-2707 sediment core (*39*) with age model by Waelbroeck *et al.* (*80*). The curve is a B-Spline fit 10 dec. Blue ribbons at the bottom indicate the time of the main supraregional "cold events" described in the literature (see the main text). Vertical scales in (B), (G), and (H) are inverted to facilitate visual comparison.

Millennial-scale changes

Our record shows changes in dust deposition rates at supracentennial to millennial scales, defined by the following: (i) a repetitive pattern with a dominant period of ~1.25 ka; (ii) four intervals of dust deposition minima occurring at 4.7 to 4.6, 3.5 to 3.2, 2.3 to 1.9, and 1.3 to 1.0 ka BP, all of them preceded by a long interval of dust decline, lasting one century or longer; and (iii) a series of dust deposition maxima at 4.3, 3.8, 2.8, 2.4, and 1.5 ka BP, typically preceded by rapid increases in dust fluxes. These features need to be considered within the North Atlantic long-term climate variability, which exerts a strong influence on winds and precipitation patterns over both western Africa and Western Europe and thus can induce changes in dust availability, atmospheric transport, and deposition.

Specifically, the four dust minima episodes (including their respective preceding intervals of rapid dust reduction) were contemporaneous with warm episodes in the tropical eastern North Atlantic, as recorded both at the sea surface (*39*) (Fig. 4H) and at intermediate depths (Eastern North Atlantic Central Water) (*46*) (Fig. 4G). Those conditions probably promoted the prevailing cool and humid conditions in subtropical western Africa, comparable to present-day positive precipitation anomalies that occur during warm phases of the Atlantic Multidecadal Oscillation and subsequent decline in Saharan dust production (*47*). At higher latitudes in the North Atlantic, our dust minima episodes correlate with (i) warm sea surface intervals in the North Atlantic Current (*48*–*50*), (ii) increased strength of the Iceland-Scotland Overflow Water (*51*) (Fig. 4B), and (iii) accelerated rates of subpolar Atlantic deep water formation (*52*). All these features point to strong Atlantic Meridional Overturning Circulation (AMOC) and a low LTG in the Northern Hemisphere. Figure 4D shows how changes in LTG at century scales remarkably mimic the Saharan dust influxes. Under those conditions, the intensity of surface westerlies across the North Atlantic onto Europe and the Mediterranean should weaken, and associated winter storm tracks would shift southward, increasing rainfall in northern Africa and the southwestern Mediterranean. It can also explain the humid winters and cool summers reported for those areas and times (*10*, *53*).

The North Atlantic ocean-atmosphere features that characterize intervals of low Saharan dust fluxes change to the opposite conditions during episodes of high (or rapidly increasing) dust influx. These become defined by the following: (i) cooling, freshening, and weakening of the subpolar gyre; (ii) advance of sea ice limiting deep convection in the northwestern Atlantic; (iii) reduced AMOC strength; (iv) intensification of the westerlies; and (v) weakening of the summer monsoon. Those conditions can be considered as typical of the so-called "Late Holocene cold events" in the Northern Hemisphere, defined as multidecadal- to century-scale climate episodes that have been extensively detected in both marine and terrestrial paleoclimate records, but whose origin, precise timing, progression, and spatial extension are still debated. Among these, probably the most relevant and best constrained are the 4.2 ka BP event (*54*, *55*), the 2.8 ka BP event (*56*, *57*), and the Dark Ages Cold Period that occurred around 1.5 ka BP (*58*). The remarkable coincidence between those cold events and the most prominent positive dust spikes points toward a close relationship between dust and climate in the last millennia that merits further discussion.

Dust-climate feedbacks and the Late Holocene cold events

Late Holocene cold events are often considered as abrupt climate changes because of their short duration and large impact. Decreased solar activity (the so-called Grand Solar Minima) has been hypothesized to be the main driver of those changes (*59*–*61*), although other causes could have been responsible for some of the events, including freshwater pulses into the North Atlantic from ice melting (*50*), volcanic activity (*62*), or spontaneous internal processes (*63*, *64*). Whatever the triggering factor, strong climate feedbacks must have occurred in all cases. Among them, dust feedbacks could play a relevant role, which has been poorly explored however, partly owing to the scarcity of reliable proxy dust records, as well as to the still incomplete understanding of radiative roles of atmospheric mineral dust, even in modern-day climate. Desert dust affects Earth's global energy balance in various ways, including by scattering and absorbing radiation, serving as a nuclei for cloud formation, and fertilizing marine and terrestrial ecosystems (*1*). Because these processes include both positive and negative forcing, which, in addition, strongly vary spatially, the net radiative influence is difficult to calculate, and climate models show large associated uncertainties (*65*). Despite that, past increases in atmospheric dust loading have been hypothesized to produce a substantial negative radiative forcing of the climate system, contributing, for instance, to cool climate during the glacial periods (*28*, *30*). Very little attention has been paid, however, to dust-climate feedback during Late Holocene cold events, and our record sheds new light on this topic.

Our record shows that dust deposition maxima are broadly contemporaneous with cold events in the Late Holocene. However, those peaks in dust deposition were typically preceded by hundreds of years during which dust influx increased progressively and intensely. This is the case of the rapid dust increases that occurred in the intervals 4.6 to 4.3, 3.2 to 2.8, and 1.9 to 1.5 ka BP, which respectively preceded global climate events occurring at ~4.2, ~2.8, and ~1.5 ka BP.

Because these periods mimic the trend shown by the LTG and other ocean and atmosphere variables (Fig. 4), a gradual climate cooling must have existed before the abrupt onset of each cold event. These "dust preludes" point toward the key question of whether abrupt Late Holocene climate changes resulted from unexpected and rapid triggering factors such as an abrupt decrease in solar irradiance, an intense volcanism, or a spontaneous internal process. Although our record does not discard abrupt triggering, it suggests that the climate system gradually moved toward cooler conditions before the onset of abrupt change, probably generating more sensitive conditions for it. These "dust preludes" also point toward a relevant role of dust feedbacks in the gradual enhancement of such conditions preceding climate abrupt events. We hypothesize that increased negative radiative forcing from increased dust emissions could enhance the cooling trend, thus leading to more intense dust emissions, thereby accelerating the cooling.

If our interpretation of a causal link between enhanced Saharan dust fluxes and cooling events in the Holocene is correct, it suggests that the dust-climate effect involves net cooling. This is apparently at odds with recent suggestions that climate models typically underrepresent the coarse dust fraction, which, if properly included, would produce slight atmospheric warming (*66*). While the connection between dust fluxes and cooling events in our study remains somewhat tentative, this apparent contradiction may imply that climate models inadequately capture some dust-climate feedbacks, a topic that clearly merits further detailed investigation.

Five millennia of Saharan dust in a stalagmite

In conclusion, $^{87}Sr/^{86}Sr$ ratios in speleothems provide a powerful proxy for past aeolian dust fluxes in areas subject to dust deposition,

if the isotopic signal of mineral dust can be distinguished from those of other sources of strontium by cave system monitoring. In this work, $^{87}Sr/^{86}Sr$ measurements along a Late Holocene stalagmite from northern Spain (43°N) provide a first quantitative reconstruction of mid- to long-term changes in Saharan dust accumulation in Western Europe over four millennia of the Late Holocene (4.9 to 0.9 ka BP).

Changes in Saharan dust fluxes detected in speleothem Buda-100 reflect broad changes in dust source areas, to the detriment of changes in regional dust transport or deposition. This hypothesis is supported by the broad correlation with previous dust records from Africa and the Atlantic (despite different resolutions) and by the coherence of the dust flux patterns when framed in the supraregional atmosphere-ocean evolution of the North Atlantic and Africa. Also, the present-day sensitivity of Iberia to Saharan dust fluxes (fig. S2) and the low influence of local hydroclimate changes on mid- and long-dust fluxes over Iberia during the last millennia (fig. S3) give additional strength to interpretations.

In the long term, Saharan dust fluxes show a net (but not monotonic) increase through the Late Holocene, with rates varying from 30 to 80% of current values, always exceeding those of the AHP (~6 ka BP). This long-term increase is consistent with the progressive desertification of large areas of northwestern Africa since the demise of the AHP and is a response to the gradual strengthening of latitudinal climate gradients in the Northern Hemisphere.

Superimposed on the large-scale positive trend in Saharan dust flux, broad quasi-periodic changes occurred at centennial to millennial scales, in which episodes of low (4.7 to 4.6, 3.5 to 3.2, 2.3 to 1.9, and 1.3 to 1.0 ka BP) and high dust deposition (4.4 to 3.8, 2.9 to 2.4, and 1.8 to 1.4 ka BP) alternated. Those variations were clearly related to North Atlantic long-term climate variability, with higher dust fluxes coinciding with (i) cooling, freshening, and weakening of the subpolar gyre; (ii) advancing of sea ice (in turn hampering deep convection in NW Atlantic); (iii) weakening of the AMOC; (iv) intensification of westerlies and northward shift of storm tracks in mid-latitudes; and (v) weakening of the summer monsoon. The opposite conditions existed during periods of low dust fluxes.

Episodes of maximum dust flux coincide with well-known cold events of the Late Holocene, which are often considered as abrupt climate changes due to their large impact, short duration, and sudden triggering. Our paleorecord indicates, however, that these events were preceded by intervals of increased dust fluxes lasting hundreds of years. Those "dust preludes" suggest that changes in the climate system occurred well before the trigger, whatever it was (e.g., solar minima, volcanism, ice melt, and spontaneous internal processes). In summary, climatic conditions gradually changed toward a higher latitudinal gradient and lower temperatures, conditions that apparently increased the sensitivity of the climate system to abrupt change.

Because changes in Saharan dust fluxes not only depend on climate but also influence climate in various ways, reconstructions of past fluxes through time are critical to investigate climate-dust feedbacks, at appropriate time scales. This paper contributes to this challenge, but more important, it will stimulate new research avenues for further exploration of a key element of the climate system.

MATERIALS AND METHODS

Samples and study site

This study focused on Buda-100 (fig. S1), a cylindrical (4 to 6 cm thick) and elongated (~117 cm long) calcite stalagmite, which was reconstructed from several broken pieces found in Buda Hall, an isolated karstic chamber of Kaite Cave (Ojo Guareña Karst Natural Monument, Burgos Province, Spain). Field work was authorized and supervised by the Government of Junta de Castilla y León. The study material is deposited in the Department of Geodynamics, Stratigraphy and Paleontology of the Complutense University of Madrid.

Kaite Cave is small (~350 m long), relatively shallow (12 to 15 m below the surface at the sampling site), and topographically isolated from the main levels of the Ojo Guareña Karst Complex. The entrance is 860 m above sea level. The sampling site is characterized by a nearly constant temperature (10.40° ± 0.04°C) that reflects the mean annual temperature outside the cave. Relative humidity exceeds 99%, and there are no relevant air currents. Seepage water is usual, with permanent dripping but seasonal modulation, with minimum rates in late summer. Speleothems are abundant, some of which are growing at the present time. The soil above the cave is a thin immature lithosol that mostly consists of weathered host rock fragments and scarce argillaceous material, and the vegetation consists of bushes and small trees. The cave is developed in a gently dipping carbonate unit of Upper Cretaceous (Coniacian) age, which consists of shallow marine, partially dolomitized limestone.

Microstratigraphic analysis of stalagmite Buda-100 reveals homogeneous features along the stalagmite, including a net dominance of columnar microcrystalline and dendritic calcite fabrics, well-defined and pervasive internal annual lamination, and no relevant stratigraphic disruptions, i.e., hiatal surfaces. These features indicate that physicochemical conditions during stalagmite growth remained broadly stable and that large changes in cave environment, dripping conditions, and epikarst and soil processes that could affect the $^{87}Sr/^{86}Sr$ record did not occur.

Strontium isotope measurements

$^{87}Sr/^{86}Sr$ analyses were performed on 101 speleothem subsamples from Buda-100, including nine pairs of samples extracted from approximately the same stratigraphic levels to check for replicability. Each sample (~0.01 g) was microdrilled carefully from the stalagmite growth axis. Similar sample weight was used to analyze the host rock and present-day speleothem precipitates. Following dissolution of the carbonate samples in 1 M HNO_3, strontium was chemically separated for isotope measurements using calibrated 1-ml Sr-spec resin columns to remove calcium, rubidium, and other trace elements (*67*). All geochemical work was performed in high efficiency particulate air filtered (HEPA) laminar flow hoods at the National Centre for Isotope Geochemistry (NCIG), University College Dublin, Ireland. The water samples (local rainfall and drip water) were simply evaporated and redissolved before loading on the ion exchange columns. The soil samples were leached using deionized H_2O as described in table S1.

Following ion-exchange chromatography, the separated Sr fraction was analyzed by thermal ionization mass spectrometry using a Thermo Fisher Scientific Triton multicollector thermal ionization spectrometer at the NCIG. The separated Sr was loaded on degassed zone-refined Re filaments using a Ta-oxide activator before analysis of $^{87}Sr/^{86}Sr$ ratios in the spectrometer. Sr isotope ratios were corrected by the software for mass bias using a $^{86}Sr/^{88}Sr$ ratio of 0.1194. Following standard analytical protocols for Sr isotope analyses, the NIST SRM 987 isotopic standard was analyzed repeatedly over the course of this study and gave a value of 0.7102616 ± 0.0000080 (quoted uncertainty in the last two digits is 2σ around the mean,

based on 16 separate analyses over ca. 2 years). Total procedural blanks for Sr that includes all of the dissolution, separation, and loading procedures are typically <1 μg of Sr and are negligible in comparison to the amounts of Sr (400 μg) analyzed in the samples, and no blank corrections were applied. Nine replicate subsamples were retrieved from some stratigraphic levels to check for consistency of results and reproducibility (fig. S1B). A small part of each subsample was also analyzed for strontium elemental concentration. Measured $^{87}Sr/^{86}Sr$ ratios for stalagmite Buda-100 (Fig. 2 and fig. S1) vary between 0.70773 and 0.70817 and show a noteworthy variability that defines consistent changes through its internal stratigraphy, with well-defined trends and patterns that should reflect nonstochastic processes.

In addition, five samples of dusty rainfall were collected in October 2020 during a Saharan dust outbreak and analyzed using a Phoenix multicollector thermal ionization mass spectrometer in the Center for Geochronology and Isotope Geochemistry, Complutense University of Madrid, Spain. The mean $^{87}Sr/^{86}Sr$ value for the isotopic standard NIST SRM 987 measured during the analysis was 0.710246 ± 0.000015 (n = 11).

Absolute age-dating

Speleothem chronology was based on 15 ^{230}Th age-dates obtained using multicollector inductively coupled plasma–mass spectrometry at the University of Minnesota, USA, following the methods referred to in the Supplementary Materials. Age-dating results, summarized in table S2, show a coherent stratigraphic order, with no outliers. Most data were already presented in (*45*). Software StalAge (*68*) was used for establishing chronologies (fig. S2). The age model and microstratigraphic analysis indicate nearly homogeneous growth rates for the stalagmite, covering the time interval between 4.9 and 0.9 ka BP.

$^{87}Sr/^{86}Sr$ model for paleodust reconstruction

The model calculates past dust deposition rates ($g{\cdot}m^{-2}{\cdot}year^{-1}$) in the cave region from $^{87}Sr/^{86}Sr$ ratio of age-dated samples of speleothem calcite.

Scientific rationale

Because strontium isotopes do not fractionate significantly from geological or mass-dependent biological processes, and the ratios have, in any case, been corrected for mass-dependent fractionation using the natural $^{88}Sr/^{86}Sr$ ratio as outlined above, the $^{87}Sr/^{86}Sr$ isotope ratio of speleothem can be used as a natural tracer of strontium sources. Sr substitutes for Ca in the calcite lattice during speleothem growth (*22*), and the $^{87}Sr/^{86}Sr$ ratio of the formed calcite should equal the $^{87}Sr/^{86}Sr$ ratio of the drip water from which it derives, which, in turn, results in the combination of the $^{87}Sr/^{86}Sr$ ratio of the different sources of strontium (*23*–*26*). In Kaite Cave, currently precipitating calcite and drip waters have a similar $^{87}Sr/^{86}Sr$ ratio (mean: 0.70835 for calcite and 0.70834 for drip water; see table S1). These ratios result from a combination of strontium of different provenance that feed drip waters, each source with a specific $^{87}Sr/^{86}Sr$ ratio. The provenance can be both internal (cave host rock) and external (sea spray and continental mineral dust).

We recognize that $^{87}Sr/^{86}Sr$ ratios measured in speleothem calcite, for both ancient and present-day samples, are likely to show some "tailing effect" reflecting the relatively slow weathering kinetics of silicate-dominated dust; i.e., they do not reflect the amount of dust accumulated above the cave during a red-rain event or during a "dusty year." Instead, they should reflect an average value of the dust accumulated during over several years or to a few decades. This "tailing effect" can explain the smoothness of our $^{87}Sr/^{86}Sr$ curve, which contrasts with, for example, the notably noisier dust paleorecords of ice cores, which more immediately reflect instantaneous deposition.

Input data

The model is based on $^{87}Sr/^{86}Sr$ isotope ratios and strontium concentration data of the various strontium sources that feed cave drip waters and present-day speleothems. These sources include the cave host rock (internal source) and sea spray and continental mineral dust (external sources).

Cave host rock is a Late Cretaceous marine limestone, which yields an average $^{87}Sr/^{86}Sr$ ratio of 0.70739 (table S1). The data are consistent with expected values for the type of geological material and age (*69*). Strontium provided by the host rock derives from carbonate dissolution by meteoric water, which occurs in the lithosol and the epikarst.

Sea spray contributes with strontium from marine sea salt aerosols. Sea salt from North Atlantic has a $^{87}Sr/^{86}Sr$ ratio of 0.709175 (*70*). We have found similar values in rainfall water assumed to be "clean," i.e., with very low influence of mineral dust (table S1). Sea salt is continuously transported to the area from the Atlantic by westerlies. The amount of sea salt that reaches Kaite area averages 4.3 ± 0.1 g m^{-2} $year^{-1}$ and has been estimated on the basis of rainfall chlorine measured during the 2004–2011 period in the frame of a long-term monitoring program we performed in Kaite Cave. Sea salt deposition rates are moderate despite the relative proximity of the sea, probably because of the shadow effect of the Cantabrian Mountains.

Continental mineral dust input occurs in the cave area mostly by wet deposition after Saharan dust outbreak events. Aeolian dust arriving to northern Iberia has its main sources in southern Algeria and northern Mali, in the western coast of northern Africa (Western Sahara, western Mauritania, Atlas foothills), and, to a lesser extent, in Argelia and Tunisia (*18*, *19*). All these zones are included in the so-called Western North African preferential dust source area (Western PSA) (*20*) (Fig. 1). Dust from that PSA is characterized by high radiogenic $^{87}Sr/^{86}Sr$ ratios (*18*, *71*), due to provenance areas dominated by Precambrian and lower Paleozoic massifs. A second broad primary source of Saharan dust is the Central North African PSA (Fig. 1), located mainly in Niger and Chad, which could also contribute subordinately to dust fluxes to southwestern Europe (*19*) and is also less $^{87}Sr/^{86}Sr$ radiogenic than the Western PSA (*20*).

For calculations, we consider average $^{87}Sr/^{86}Sr$ ratios of Saharan dust in the area to be between 0.7279 and 0.7186, which correspond to the Western and Central North African PSAs average ratios (*20*) and are taken as a maximum and a minimum estimate for dust $^{87}Sr/^{86}Sr$. Saharan dust deposited in the Canary Islands, which shows an average $^{87}Sr/^{86}Sr$ of 0.72523, is considered for calculations as a best estimate for dust source isotopic composition (*18*). Current mineral dust deposition rate in inland northern Spain is 2 to 5 g m^{-2} $year^{-1}$, according to some climate models (*72*–*74*), although some estimate 5 to 10 g m^{-2} $year^{-1}$ (*32*). Surface measurements in neighboring regions suggest rates in the limit between those two ranges (*17*, *75*–*77*). Integrating all available data, we obtained a best estimate of 4.4 ± 1.1 g m^{-2} $year^{-1}$ for present-day rates of Saharan dust deposition in the study area, with an average concentration of strontium of 95 parts per million (*18*, *71*).

The model also requires input data of $^{87}Sr/^{86}Sr$ ratios in present-day drip waters and speleothems. As mentioned above, currently precipitating calcite and drip waters have, as expected, similar $^{87}Sr/^{86}Sr$ ratios (table S1).

Calculations

The model operates in two steps (see Supplementary Material Spreadsheet). The first step is a simple mass balance model to quantitatively estimate the present-day influence of Saharan dust on the speleothem $^{87}Sr/^{86}Sr$ ratio. It calculates the relative contribution of external and internal strontium sources to present-day drip waters and speleothem carbonate. Then, the relative contributions of mineral dust and salt spray are calculated on the basis of their different accumulation rates, $^{87}Sr/^{86}Sr$ ratios, and strontium concentrations.

The second step calculates past dust deposition rates in the study area from $^{87}Sr/^{86}Sr$ ratios measured in samples of known ages of the speleothem and considers the contribution of mineral dust to speleothem $^{87}Sr/^{86}Sr$ ratio in present-day conditions, as calculated in step 1. The model considers that changes of $^{87}Sr/^{86}Sr$ ratio through time recorded in the stalagmite are the reflection of changes in the amount of Saharan dust deposited above the cave, at the expense of the other sources, whose influence is assumed to be very small. In the case of sea spray, deposition rates are expected to be very homogeneous at supradecadal or longer scales during the Late Holocene (*78*). Even if a large variation in sea salt deposition occurred, it would not be able to explain the observed variation in speleothem $^{87}Sr/^{86}Sr$. In the case of host rock, and because it contributes to most of the speleothem strontium, unrealistic large changes in water-rock interaction rates would be needed to generate significant changes in the speleothem $^{87}Sr/^{86}Sr$ ratio, and these would be clearly recorded in variations in the strontium concentration of the speleothem calcite and/or in the speleothem growth rates, none of which are observed (fig. S2). Furthermore, such hypothetical changes in water-rock interaction would, in turn, require large changes in net rates of epikarst water recharge, but these have been shown to change only moderately in the area over long time scales (centennial or longer scales) (*45*). For these reasons, the relative contributions of sea spray and host rock to speleothem strontium are kept fixed in our calculations to the present-day values and are assumed not to vary through time. The calculations also assume that the $^{87}Sr/^{86}Sr$ of Saharan dust, sea salt, and host rock do not vary through time for the considered time interval.

Uncertainties

The main uncertainty in our dust flux calculations arises from present-day estimates of Saharan dust deposition rates in central to northern Iberia (4.4 ± 1.1 g m^{-2} year^{-1}), as this value determines the present-day contribution of dust Sr to speleothem Sr and gives a calibration point for past variations in dust deposition. Possible changes in the relative contributions of different dust source areas to the $^{87}Sr/^{86}Sr$ ratios of the deposited dust are a secondary source of uncertainty that could influence our calculation of past dust deposition rate. Uncertainties associated to changes in relative dust source contribution (e.g., Western versus Central PSAs relative input) are in the range between 0.01 and 0.1 g m^{-2} year^{-1}, clearly much less than the reconstructed variability in dust deposition rates (Fig. 2). We have considered both aspects (present-day dust deposition rate and past changes in the relative contribution of dust sources) to get maximum and minimum estimates of dust deposition rates. To calculate the minimum (or maximum) dust deposition values, we used present-day lowest (or highest) dust flux estimate and the maximum (or minimum) $^{87}Sr/^{86}Sr$ value for dust composition (Fig. 2).

SUPPLEMENTARY MATERIALS

Supplementary material for this article is available at http://advances.sciencemag.org/cgi/content/full/7/26/eabe6102/DC1

REFERENCES AND NOTES

1. K. S. Carslaw, O. Boucher, D. V. Spracklen, G. W. Mann, J. G. L. Rae, S. Woodward, M. Kulmala, A review of natural aerosol interactions and feedbacks within the Earth system. *Atmos. Chem. Phys.* **10**, 1701–1737 (2010).
2. F. Solmon, M. Mallet, N. Elguindi, F. Giorgi, A. Zakey, A. Konaré, Dust aerosol impact on regional precipitation over western Africa, mechanisms and sensitivity to absorption properties. *Geophys. Res. Lett.* **35**, 1–6 (2008).
3. M. Kotsyfakis, S. G. Zarogiannis, E. Patelarou, The health impact of Saharan dust exposure. *Int. J. Occup. Med. Environ. Health* **32**, 749–760 (2019).
4. P. Ginoux, J. M. Prospero, T. E. Gill, N. C. Hsu, M. Zhao, Global-scale attribution of anthropogenic and natural dust sources and their emission rates based on MODIS Deep Blue aerosol products. *Rev. Geophys.* **50**, 1–36 (2012).
5. O. Boucher, D. Randall, P. Artaxo, C. Bretherton, G. Feingold, P. Forster, V.-M. Kerminen, Y. Kondo, H. Liao, U. Lohmann, P. Rasch, S. K. Satheesh, S. Sherwood, B. Stevens, X. Y. Zhang, in *Climate Change 2013 the Physical Science Basis: Working Group I Contribution to the Fifth Assessment Report of the Intergovernmental Panel on Climate Change*, T. F. Stocker, D. Qin, G.-K. Plattner, M. Tignor, S. K. Allen, J. Boschung, A. Nauels, Y. Xia, Eds. (Cambridge University Press, New York, 2013), pp. 571–658.
6. C. Wu, Z. Lin, X. Liu, The global dust cycle and uncertainty in CMIP5 (coupled model intercomparison project phase 5) models. *Atmos. Chem. Phys.* **20**, 10401–10425 (2020).
7. C. Wang, S. Dong, A. T. Evan, G. R. Foltz, S. K. Lee, Multidecadal covariability of north atlantic sea surface temperature, African dust, Sahel Rainfall, and Atlantic hurricanes. *J. Clim.* **25**, 5404–5415 (2012).
8. T. M. Shanahan, N. P. Mckay, K. A. Hughen, J. T. Overpeck, B. Otto-Bliesner, C. W. Heil, J. King, C. A. Scholz, J. Peck, The time-transgressive termination of the African humid period. *Nat. Geosci.* **8**, 140–144 (2015).
9. P. Sabatier, M. Nicolle, C. Piot, C. Colin, M. Debret, D. Swingedouw, Y. Perrette, M. C. Bellingery, B. Chazeau, A. L. Develle, M. Leblanc, C. Skonieczny, Y. Copard, J. L. Reyss, E. Malet, I. Jouffroy-Bapicot, M. Kelner, J. Poulenard, J. Didier, F. Arnaud, B. Vannière, Past African dust inputs in the western Mediterranean area controlled by the complex interaction between the Intertropical Convergence Zone, the North Atlantic Oscillation, and total solar irradiance. *Clim. Past* **16**, 283–298 (2020).
10. C. Zielhofer, H. von Suchodoletz, W. J. Fletcher, B. Schneider, E. Dietze, M. Schlegel, K. Schepanski, B. Weninger, S. Mischke, A. Mikdad, Millennial-scale fluctuations in Saharan dust supply across the decline of the African Humid Period. *Quat. Sci. Rev.* **171**, 119–135 (2017).
11. H. M. Clifford, N. E. Spaulding, A. V. Kurbatov, A. More, E. V. Korotkikh, S. B. Sneed, M. Handley, K. A. Maasch, C. P. Loveluck, J. Chaplin, M. McCormick, P. A. Mayewski, A 2000 year Saharan dust event proxy record from an ice core in the European Alps. *J. Geophys. Res. Atmos.* **124**, 12882–12900 (2019).
12. D. McGee, P. B. deMenocal, G. Winckler, J. B. W. Stuut, L. I. Bradtmiller, The magnitude, timing and abruptness of changes in North African dust deposition over the last 20,000 yr. *Earth Planet. Sci. Lett.* **371–372**, 163–176 (2013).
13. J. L. Middleton, S. Mukhopadhyay, C. H. Langmuir, J. F. McManus, P. J. Huybers, Millennial-scale variations in dustiness recorded in Mid-Atlantic sediments from 0 to 70 ka. *Earth Planet. Sci. Lett.* **482**, 12–22 (2018).
14. S. Mulitza, D. Heslop, D. Pittauerova, H. W. Fischer, I. Meyer, J. B. Stuut, M. Zabel, G. Mollenhauer, J. A. Collins, H. Kuhnert, M. Schulz, Increase in African dust flux at the onset of commercial agriculture in the Sahel region. *Nature* **466**, 226–228 (2010).
15. J. Adkins, P. deMenocal, G. Eshel, The "African humid period" and the record of marine upwelling from excess 230Th in Ocean Drilling Program Hole 658C. *Paleoceanography* **21**, PA4203 (2006).
16. P. Demenocal, J. Ortiz, T. Guilderson, J. Adkins, M. Sarnthein, L. Baker, M. Yarusinsky, Abrupt onset and termination of the African Humid Period: Rapid climate responses to gradual insolation forcing. *Quat. Sci. Rev.* **19**, 347–361 (2000).
17. S. Guerzoni, E. Molinaroli, R. Chester, Saharan dust inputs to the western Mediterranean Sea: Depositional. *Deep Res. II* **44**, 631–654 (1997).
18. D. Scheuvens, L. Schütz, K. Kandler, M. Ebert, S. Weinbruch, Bulk composition of northern African dust and its source sediments—A compilation. *Earth Sci. Rev.* **116**, 170–194 (2013).
19. P. Salvador, S. Alonso-Pérez, J. Pey, B. Artíñano, J. J. De Bustos, A. Alastuey, X. Querol, African dust outbreaks over the western Mediterranean Basin: 11-year characterization of atmospheric circulation patterns and dust source areas. *Atmos. Chem. Phys.* **14**, 6759–6775 (2014).
20. A. M. Jewell, N. Drake, A. J. Crocker, N. L. Bakker, T. Kunkelova, C. S. Bristow, M. J. Cooper, J. A. Milton, P. S. Breeze, P. A. Wilson, Three North African dust source areas and their geochemical fingerprint. *Earth Planet. Sci. Lett.* **554**, 116645 (2021).
21. S. Castillo, A. Alastuey, E. Cuevas, X. Querol, A. Avila, Quantifying dry and wet deposition fluxes in two regions of contrasting African influence: The NE Iberian Peninsula and the Canary Islands. *Atmosfera* **8**, 86 (2017).

22. I. J. Fairchild, P. C. Treble, Trace elements in speleothems as recorders of environmental change. *Quat. Sci. Rev.* **28**, 449–468 (2009).
23. A. Ayalon, M. Bar-Matthews, A. Kaufman, Petrography, strontium, barium and uranium concentrations, and strontium and uranium isotope ratios in speleothems as palaeoclimatic proxies: Soreq Cave, Israel. *The Holocene* **9**, 715–722 (1999).
24. A. Goede, M. McCulloch, F. McDermott, C. Hawkesworth, Aeolian contribution to strontium and strontium isotope variations in a tasmanian speleothem. *Chem. Geol.* **149**, 37–50 (1998).
25. J. L. Oster, I. P. Montañez, T. P. Guilderson, W. D. Sharp, J. L. Banner, Modeling speleothem δ13C variability in a central Sierra Nevada cave using 14C and 87Sr/86Sr. *Geochim. Cosmochim. Acta* **74**, 5228–5242 (2010).
26. A. Frumkin, M. Stein, The Sahara-East Mediterranean dust and climate connection revealed by strontium and uranium isotopes in a Jerusalem speleothem. *Earth Planet. Sci. Lett.* **217**, 451–464 (2004).
27. B. E. Wortham, C. I. Wong, L. C. R. Silva, D. McGee, I. P. Montañez, E. Troy Rasbury, K. M. Cooper, W. D. Sharp, J. J. G. Glessner, R. V. Santos, Assessing response of local moisture conditions in central Brazil to variability in regional monsoon intensity using speleothem 87Sr/86Sr values. *Earth Planet. Sci. Lett.* **463**, 310–322 (2017).
28. P. O. Hopcroft, P. J. Valdes, On the role of dust-climate feedbacks during the mid-Holocene. *Geophys. Res. Lett.* **46**, 1612–1621 (2019).
29. S. Egerer, M. Claussen, C. Reick, T. Stanelle, The link between marine sediment records and changes in Holocene Saharan landscape: Simulating the dust cycle. *Clim. Past* **12**, 1009–1027 (2016).
30. S. Albani, N. M. Mahowald, G. Winckler, R. F. Anderson, L. I. Bradtmiller, B. Delmonte, R. François, M. Goman, N. G. Heavens, P. P. Hesse, S. A. Hovan, S. G. Kang, K. E. Kohfeld, H. Lu, V. Maggi, J. A. Mason, P. A. Mayewski, D. McGee, X. Miao, B. L. Otto-Bliesner, A. T. Perry, A. Pourmand, H. M. Roberts, N. Rosenbloom, T. Stevens, J. Sun, Twelve thousand years of dust: The Holocene global dust cycle constrained by natural archives. *Clim. Past* **11**, 869–903 (2015).
31. R. H. Williams, D. McGee, C. W. Kinsley, D. A. Ridley, S. Hu, A. Fedorov, I. Tal, R. W. Murray, P. B. deMenocal, Glacial to Holocene changes in trans-Atlantic Saharan dust transport and dust-climate feedbacks. *Sci. Adv.* **2**, e1600445 (2016).
32. Y. H. Lee, K. Chen, P. J. Adams, Development of a global model of mineral dust aerosol microphysics. *Atmos. Chem. Phys.* **9**, 2441–2458 (2009).
33. P. DeMenocal, J. Ortiz, T. Guilderson, M. Sarnthein, Coherent high- and low-latitude climate variability during the holocene warm period. *Science* **288**, 2198–2202 (2000).
34. J. E. Tierney, F. S. R. Pausata, P. B. De Menocal, Rainfall regimes of the Green Sahara. *Sci. Adv.* **3**, e1601503 (2017).
35. J. A. Collins, M. Prange, T. Caley, L. Gimeno, B. Beckmann, S. Mulitza, C. Skonieczny, D. Roche, E. Schefuß, Rapid termination of the African Humid Period triggered by northern high-latitude cooling. *Nat. Commun.* **8**, 1372 (2017).
36. B. Damnati, Holocene lake records in the Northern Hemisphere of Africa. *J. Afr. Earth Sci.* **31**, 253–262 (2000).
37. C. Hély, A. M. Lézine, A. Ballouche, P. Cour, D. Duzer, P. Guinet, S. Jahns, J. Maley, A. M. Mercuri, A. Pons, J. C. Ritchie, U. Salzmann, E. Schulz, M. Van Campo, M. P. Waller, Holocene changes in African vegetation: Tradeoff between climate and water availability. *Clim. Past* **10**, 681–686 (2014).
38. M. C. Gatto, A. Zerboni, Holocene supra-regional environmental changes as trigger for major socio-cultural processes in northeastern Africa and the Sahara. *Afr. Archaeol. Rev.* **32**, 301–333 (2015).
39. S. Weldeab, D. W. Lea, R. R. Schneider, N. Andersen, Centennial scale climate instabilities in a wet early Holocene West African monsoon. *Geophys. Res. Lett.* **34**, L24702 (2007).
40. Y. Wang, H. Cheng, R. L. Edwards, Y. He, X. Kong, Z. An, J. Wu, M. J. Kelly, C. A. Dykoski, X. Li, The holocene Asian monsoon: Links to solar changes and North Atlantic climate. *Science* **308**, 854–857 (2005).
41. S. Weldeab, V. Menke, G. Schmiedl, The pace of East African monsoon evolution during the Holocene. *Geophys. Res. Lett.* **41**, 1724–1732 (2014).
42. G. H. Haug, K. A. Hughen, D. M. Sigman, L. C. Peterson, U. Röhl, Southward migration of the Intertropical Convergence Zone through the Holocene. *Science* **293**, 1304–1309 (2001).
43. C. C. Routson, N. P. McKay, D. S. Kaufman, M. P. Erb, H. Goosse, B. N. Shuman, J. R. Rodysill, T. Ault, Mid-latitude net precipitation decreased with Arctic warming during the Holocene. *Nature* **568**, 83–87 (2019).
44. L. M. Baldini, J. U. L. Baldini, F. McDermott, P. Arias, M. Cueto, I. J. Fairchild, D. L. Hoffmann, D. P. Mattey, W. Müller, D. C. Nita, R. Ontañón, C. Garciá-Moncó, D. A. Richards, North Iberian temperature and rainfall seasonality over the Younger Dryas and Holocene. *Quat. Sci. Rev.* **226**, 105998 (2019).
45. J. A. Cruz, M. J. Turrero, J. O. Cáceres, A. Marín-Roldán, A. I. Ortega, A. Garralón, L. Sánchez, P. Gómez, M. B. Muñoz-García, R. L. Edwards, J. Martín-Chivelet, Long-term hydrological changes in northern Iberia (4.9–0.9 ky BP) from speleothem Mg/Ca ratios and cave monitoring (Ojo Guareña Karst Complex, Spain). *Environ. Earth Sci.* **74**, 7741–7753 (2015).
46. A. Morley, Y. Rosenthal, P. DeMenocal, Ocean-atmosphere climate shift during the mid-to-late Holocene transition. *Earth Planet. Sci. Lett.* **388**, 18–26 (2014).
47. G. R. Foltz, M. J. McPhaden, Trends in Saharan dust and tropical Atlantic climate during 1980-2006. *Geophys. Res. Lett.* **35**, L20706 (2008).
48. B. Risebrobakken, E. Jansen, C. Andersson, E. Mjelde, K. Hevrøy, A high-resolution study of Holocene paleoclimatic and paleoceanographic changes in the Nordic Seas. *Paleoceanography* **18**, 1017 (2003).
49. M. Moros, K. Emeis, B. Risebrobakken, I. Snowball, A. Kuijpers, J. McManus, E. Jansen, Sea surface temperatures and ice rafting in the Holocene North Atlantic: Climate influences on northern Europe and Greenland. *Quat. Sci. Rev.* **23**, 2113–2126 (2004).
50. M. Moros, J. T. Andrews, D. D. Eberl, E. Jansen, Holocene history of drift ice in the northern North Atlantic: Evidence for different spatial and temporal modes. *Paleoceanography* **21**, PA2017 (2006).
51. T. L. Mjell, U. S. Ninnemann, T. Eldevik, H. K. F. Kleiven, Holocene multidecadal- to millennial-scale variations in Iceland-Scotland overflow and their relationship to climate. *Paleoceanography* **30**, 558–569 (2015).
52. D. W. Oppo, J. F. McManus, J. L. Cullen, Deepwater variability in the Holocene Epoch. *Nature* **422**, 277–278 (2003).
53. J. Schirrmacher, M. Weinelt, T. Blanz, N. Andersen, E. Salgueiro, R. R. Schneider, Multi-decadal atmospheric and marine climate variability in southern Iberia during the mid- to late-Holocene. *Clim. Past* **15**, 617–634 (2019).
54. H. Weiss, Global megadrought, societal collapse and resilience at 4.2-3.9 ka BP across the Mediterranean and west Asia. *Past Glob. Chang. Mag.* **24**, 62–63 (2016).
55. M. Bini, G. Zanchetta, A. Perşoiu, R. Cartier, A. Català, I. Cacho, J. R. Dean, F. Di Rita, R. N. Drysdale, M. Finnè, I. Isola, B. Jalali, F. Lirer, D. Magri, A. Masi, L. Marks, A. M. Mercuri, O. Peyron, L. Sadori, M. A. Sicre, F. Welc, C. Zielhofer, E. Brisset, The 4.2 ka BP Event in the Mediterranean region: An overview. *Clim. Past* **15**, 555–577 (2019).
56. B. van Geel, N. A. Bokovenko, N. D. Burova, K. V. Chugunov, V. A. Dergachev, V. G. Dirksen, M. Kulkova, A. Nagler, H. Parzinger, J. van der Plicht, S. S. Vasiliev, G. I. Zaitseva, Climate change and the expansion of the Scythian culture after 850 BC: A hypothesis. *J. Archaeol. Sci.* **31**, 1735–1742 (2004).
57. C. Martin-Puertas, K. Matthes, A. Brauer, R. Muscheler, F. Hansen, C. Petrick, A. Aldahan, G. Possnert, B. Van Geel, Regional atmospheric circulation shifts induced by a grand solar minimum. *Nat. Geosci.* **5**, 397–401 (2012).
58. S. Helama, P. D. Jones, K. R. Briffa, Dark Ages Cold Period: A literature review and directions for future research. *The Holocene* **27**, 1600–1606 (2017).
59. C. J. Wu, I. G. Usoskin, N. Krivova, G. A. Kovaltsov, M. Baroni, E. Bard, S. K. Solanki, Solar activity over nine millennia: A consistent multi-proxy reconstruction. *Astron. Astrophys.* **615**, 1–13 (2018).
60. H. Wanner, J. Beer, J. Bütikofer, T. J. Crowley, U. Cubasch, J. Flückiger, H. Goosse, M. Grosjean, F. Joos, J. O. Kaplan, M. Küttel, S. A. Müller, I. C. Prentice, O. Solomina, T. F. Stocker, P. Tarasov, M. Wagner, M. Widmann, Mid- to Late Holocene climate change: An overview. *Quat. Sci. Rev.* **27**, 1791–1828 (2008).
61. G. Bond, B. Kromer, J. Beer, R. Muscheler, M. N. Evans, W. Showers, S. Hoffmann, R. Lotti-Bond, I. Hajdas, G. Bonani, Persistent solar influence on north atlantic climate during the Holocene. *Science* **294**, 2130–2136 (2001).
62. T. Kobashi, L. Menviel, A. Jeltsch-Thömmes, B. M. Vinther, J. E. Box, R. Muscheler, T. Nakaegawa, P. L. Pfister, M. Döring, M. Leuenberger, H. Wanner, A. Ohmura, Volcanic influence on centennial to millennial Holocene Greenland temperature change. *Sci. Rep.* **7**, 1441 (2017).
63. A. Klus, M. Prange, V. Varma, L. Bruno Tremblay, M. Schulz, Abrupt cold events in the North Atlantic Ocean in a transient Holocene simulation. *Clim. Past* **14**, 1165–1178 (2018).
64. S. Drijfhout, E. Gleeson, H. A. Dijkstra, V. Livina, Spontaneous abrupt climate change due to an atmospheric blocking-Sea-Ice-Ocean feedback in an unforced climate model simulation. *Proc. Natl. Acad. Sci. U.S.A.* **110**, 19713–19718 (2013).
65. J. F. Kok, D. S. Ward, N. M. Mahowald, A. T. Evan, Global and regional importance of the direct dust-climate feedback. *Nat. Commun.* **9**, 241 (2018).
66. A. A. Adebiyi, J. F. Kok, Climate models miss most of the coarse dust in the atmosphere. *Sci. Adv.* **6**, eaaz9507 (2020).
67. E. Philip Horwitz, R. Chiarizia, M. L. Dietz, A novel strontium-selective extraction chromatographic resin*. *Solvent Extr. Ion Exch.* **10**, 313–336 (1992).
68. D. Scholz, D. L. Hoffmann, StalAge - An algorithm designed for construction of speleothem age models. *Quat. Geochronol.* **6**, 369–382 (2011).
69. J. M. McArthur, R. J. Howarth, G. A. Shields, in *The Geologic Time Scale 2012*, F. M. Gradstein, J. G. Ogg, M. Schmitz, G. Ogg, Eds. (Elsevier B.V., 2012), pp. 127–144.
70. J. M. McArthur, Recent trends in strontium isotope stratigraphy. *Terra Nova* **6**, 331–358 (1994).
71. F. E. Grousset, M. Parra, A. Bory, P. Martinez, P. Bertrand, G. Shimmield, R. M. Ellam, Saharan wind regimes traced by the Sr-Nd isotopic composition of subtropical Atlantic sediments: Last Glacial Maximum vs today. *Quat. Sci. Rev.* **17**, 395–409 (1998).

72. N. M. Mahowald, A. R. Baker, G. Bergametti, N. Brooks, R. A. Duce, T. D. Jickells, N. Kubilay, J. M. Prospero, I. Tegen, Atmospheric global dust cycle and iron inputs to the ocean. *Glob. Biogeochem. Cycles* **19**, GB4025 (2005).
73. C. S. Zender, H. Bian, D. Newman, Mineral Dust Entrainment and Deposition (DEAD) model: Description and 1990s dust climatology. *J. Geophys. Res. D Atmos.* **108**, 4416 (2003).
74. P. Ginoux, M. Chin, I. Tegen, J. M. Prospero, B. Holben, O. Dubovik, S. J. Lin, Sources and distributions of dust aerosols simulated with the GOCART model. *J. Geophys. Res. Atmos.* **106**, 20255–20273 (2001).
75. A. Avila, L. Aguillaume, Monitorización y tendencias de la deposición de N en España, incluyendo polvo sahariano. *Ecosistemas* **26**, 16–24 (2017).
76. A. Avila, I. Queralt-Mitjans, M. Alarcón, Mineralogical composition of African dust delivered by red rains over northeastern Spain. *J. Geophys. Res. Atmos.* **102**, 21977–21996 (1997).
77. C. R. Lawrence, J. C. Neff, The contemporary physical and chemical flux of aeolian dust: A synthesis of direct measurements of dust deposition. *Chem. Geol.* **267**, 46–63 (2009).
78. N. M. Mahowald, J. F. Lamarque, X. X. Tie, E. Wolff, Sea-salt aerosol response to climate change: Last Glacial Maximum, preindustrial, and doubled carbon dioxide climates. *J. Geophys. Res. Atmos.* **111**, D05303 (2006).
79. A. Berger, M. F. Loutre, Insolation values for the climate of the last 10 million years. *Quat. Sci. Rev.* **10**, 297–317 (1991).
80. C. Waelbroeck, B. C. Lougheed, N. Vazquez Riveiros, L. Missiaen, J. Pedro, T. Dokken, I. Hajdas, L. Wacker, P. Abbott, J. P. Dumoulin, F. Thil, F. Eynaud, L. Rossignol, W. Fersi, A. L. Albuquerque, H. Arz, W. E. N. Austin, R. Came, A. E. Carlson, J. A. Collins, B. Dennielou, S. Desprat, A. Dickson, M. Elliot, C. Farmer, J. Giraudeau, J. Gottschalk, J. Henderiks, K. Hughen, S. Jung, P. Knutz, S. Lebreiro, D. C. Lund, J. Lynch-Stieglitz, B. Malaizé, T. Marchitto, G. Martínez-Méndez, G. Mollenhauer, F. Naughton, S. Nave, D. Nürnberg, D. Oppo, V. Peck, F. J. C. Peeters, A. Penaud, R. da C. Portilho-Ramos, J. Repschläger, J. Roberts, C. Rühlemann, E. Salgueiro, M. F. Sanchez Goni, J. Schönfeld, P. Scussolini, L. C. Skinner, C. Skonieczny, D. Thornalley, S. Toucanne, D. Van Rooij, L. Vidal, A. H. L. Voelker, M. Wary, S. Weldeab, M. Ziegler, Consistently dated Atlantic sediment cores over the last 40 thousand years. *Sci. Data* **6**, 165 (2019).
81. A. T. Evan, C. Flamant, M. Gaetani, F. Guichard, The past, present and future of African dust. *Nature* **531**, 493–495 (2016).
82. A. Sanchez-Romero, A. Sanchez-Lorenzo, J. A. González, J. Calbó, Reconstruction of long-term aerosol optical depth series with sunshine duration records. *Geophys. Res. Lett.* **43**, 1296–1305 (2016).
83. A. T. Evan, S. Mukhopadhyay, African Dust over the Northern Tropical Atlantic: 1955–2008. *J. Appl. Meteorol. Climatol.* **49**, 2213–2229 (2010).
84. N. M. Mahowald, S. Kloster, S. Engelstaedter, J. K. Moore, S. Mukhopadhyay, J. R. McConnell, S. Albani, S. C. Doney, A. Bhattacharya, M. A. J. Curran, M. G. Flanner, F. M. Hoffman, D. M. Lawrence, K. Lindsay, P. A. Mayewski, J. Neff, D. Rothenberg, E. Thomas, P. E. Thornton, C. S. Zender, Observed 20th century desert dust variability: Impact on climate and biogeochemistry. *Atmos. Chem. Phys.* **10**, 10875–10893 (2010).
85. D. Domínguez-Villar, X. Wang, H. Cheng, J. Martín-Chivelet, R. L. Edwards, A high-resolution late Holocene speleothem record from Kaite Cave, northern Spain: δ18O variability and possible causes. *Quat. Int.* **187**, 40–51 (2008).
86. J. Martín-Chivelet, M. B. Muñoz-García, R. L. Edwards, M. J. Turrero, A. I. Ortega, Land surface temperature changes in Northern Iberia since 4000yrBP, based on δ13C of speleothems. *Glob. Planet. Chang.* **77**, 1–12 (2011).
87. D. Domínguez-Villar, X. Wang, K. Krklec, H. Cheng, R. L. Edwards, The control of the tropical North Atlantic on Holocene millennial climate oscillations. *Geology* **45**, 303–306 (2017).
88. R. L. Edwards, J. H. Chen, G. J. Wasserburg, ^{238}U-^{234}U-^{230}Th-^{232}Th systematics and the precise measurement of time over the past 500,000 years. *Earth Planet. Sci. Lett.* **81**, 175–192 (1987).
89. H. Cheng, R. L. Edwards, C. C. Shen, V. J. Polyak, Y. Asmerom, J. Woodhead, J. Hellstrom, Y. Wang, X. Kong, C. Spötl, X. Wang, E. Calvin Alexander, Improvements in ^{230}Th dating, ^{230}Th and ^{234}U half-life values, and U-Th isotopic measurements by multi-collector inductively coupled plasma mass spectrometry. *Earth Planet. Sci. Lett.* **371–372**, 82–91 (2013).

Acknowledgments: We thank the facilities and permissions given by the Junta de Castilla y León (Spain) for accessing and working in the Ojo Guareña Karst Natural Monument. Thanks are extended to M. Murphy (UCD) for help with the Sr isotope measurements and A. I. Ortega (Cenieh), M. Belén Muñoz (UCM), A. Garralón (Ciemat), and L. Sanchez (Ciemat) for contributions to cave work and discussions on the paper. The collaboration of the Grupo Espeleológico Edelweiss during field work is also greatly acknowledged. We appreciate comments from the anonymous reviewers that helped us to improve the manuscript. **Funding:** This work was supported by AEI research projects CGL2013-43257-R and CGL2017-83287-R, CLIMSED UCM-910198 research group, and NSF grant 1702816 to R.L.E. J.A.C.'s work was framed within the BES-2011-049219 pre-doctoral grant of the Spanish government. **Author contributions:** J.M.-C., F.M., and J.A.C. designed the study. J.A.C. and F.M. conducted the Sr analyses. R.L.E., M.J.T., and J.M.-C. performed U-Th dating. M.J.T. led cave monitoring work. J.M.-C. and J.A.C. developed the paleodust conceptual model. J.M.-C. wrote the manuscript, with contributions from all authors. **Competing interests:** The authors declare that they have no competing interests. **Data and materials availability:** All data needed to evaluate the conclusions in the paper are present in the paper and/or the Supplementary Materials. Complete datasets are publicly accessible at www.ncdc.noaa.gov/data-access/paleoclimatology-data and www.pangaea.de.

Submitted 2 September 2020
Accepted 13 May 2021
Published 25 June 2021
10.1126/sciadv.abe6102

Citation: J. A. Cruz, F. McDermott, M. J. Turrero, R. L. Edwards, J. Martín-Chivelet, Strong links between Saharan dust fluxes, monsoon strength, and North Atlantic climate during the last 5000 years. *Sci. Adv.* **7**, eabe6102 (2021).